Physics – Uspekhi **65** (8) 852 – 863 (2022)

INSTRUMENTS AND METHODS OF INVESTIGATION PACS numbers: **07.35.+k**, **07.60.–j**, 42.79.Jq

Remote measurement of the temperature distribution on the surface of solids under high-power laser irradiation

P V Zinin, K M Bulatov, A A Bykov, Yu V Mantrova, I B Kutuza

DOI: https://doi.org/10.3367/UFNe.2021.05.038996

Contents

Abstract. The paper reviews the latest results on the application of hyperspectral imaging to measure the temperature distribution and the emissivity on the surface of solids under laser heating in diamond anvil cells. In 2016, it was proposed to use a double acousto-optic filter, which enabled obtaining a large set of experimental points on the Planck curve and achieving a high accuracy of temperature determination. Employing an acousto-optic filter also makes it possible to visualize the intensity distribution of infrared laser radiation, study melting, and measure the thermal conductivity of metals at high pressures and temperatures.

Keywords: laser heating, temperature distribution, high pressures, emissivity, thermal radiation, phase transitions, diamond anvil cells

1. Introduction

The behavior of matter under extreme conditions (high pressures and temperatures) is of interest for both fundamental and applied research [1–5]. An analysis of the behavior of minerals at high pressures and temperatures makes it possible to determine the internal structure of Earth, simulate volcanic eruptions, and study the water cycle in the mantle as well as the mechanism of movement of tectonic plates [6–8]. Currently, laser heating (LH) in high-pressure cells with diamond anvil cells (DACs) is the only experimental method for producing static extreme pressures up to 600 GPa [9] and temperatures up to 6000 K [10], and therefore it finds wide application in phase transition research [11–14] and for the synthesis of new superhard materials [15–17]. The year 2016 saw the publication of data from experiments in a high-pressure cell with diamond anvils with an embedded nanocrystalline sphere, where the pressure between the sphere and the diamond was estimated at 1 TPa [18]. The use of a high-pressure cell with toroidal diamond anvils makes it possible to achieve a pressure of 585 GPa at the center of such an anvil [19]. Experiments in the field of ultrahigh pressures are isolated, and reaching pressures above 400 GPa is the subject of intense scientific discussion [20]. Studies in which ultrahigh temperatures (> 4000 K) are obtained in high pressure cells are also rare. In particular, as a result of iron heating at 377 GPa, a temperature of 5700 K was reached, which is close to the temperature of Earth's inner core [10]. A description of experiments on heating silicate perovskite to 5257 K can be found in Ref. [21].

Among the recent striking successes achieved with the use of laser heating in high-pressure cells is the production of high-temperature superconductivity in metal hydrides [22, 23]. Further progress in high-pressure physics and Earth physics is closely related to the development of both methods for implementing the laser heating procedure itself and methods for diagnosing heated bodies, in particular, to the development of tools and methods for measuring the temperature distribution in cells with diamond anvils.

Laser heating occurs due to the absorption of infrared (IR) laser radiation in a sample located in a high-pressure cell after passing through a diamond anvil, which is transparent to laser radiation. In 1968, Taro Takahashi and William

P V Zinin, K M Bulatov, A A Bykov, Yu V Mantrova, I B Kutuza [(a)]
Scientific and Technological Center of Unique Instrumentation,
Russian Academy of Sciences,
ul. Butlerova 15, 117342 Moscow, Russian Federation
E-mail: [(a)] kutuza@mail.ru

Received 1 April 2021, revised 18 May 2021
Uspekhi Fizicheskikh Nauk **192** (8) 913 – 925 (2022)
Translated by E N Ragozin

Bassett observed a phase transition in graphite under laser heating at high pressures [24]. The first results using laser heating were published in 1974 [25]. At present, the method of laser heating in high-pressure cells is one of the main tools in the arsenal of high-pressure physics [11, 26]. With laser heating, the determination of the temperature of the sample surface is carried out by measuring the intensity of thermal radiation emitted by the sample. The spectrum of thermal radiation is usually measured with a spectrometer in a range of 600–800 nm [27]. Subsequent fitting of the measured spectrum and the theoretical curve of thermal radiation (Planck's law) makes it possible to determine the temperature of the sample upon laser heating [28].

Unfortunately, the temperature distribution over the heated area illuminated by the laser beam is highly nonuniform, and the standard method for determining the temperature in a sample gives the temperature averaged over the heated spot [26, 29, 30]. The issue of measuring the temperature distribution and producing uniform heating in high-pressure cells has become especially relevant in connection with the development of new methods for determining the velocities of acoustic waves in solids at high pressures and temperatures [31, 32]. To measure the temperature distribution on the surface of a heated sample located in a high-pressure cell, Campbell [33] developed a multispectral technique in which two-dimensional (2D) temperature mapping of a sample during laser heating in high-pressure cells was performed by simultaneously processing four images obtained in narrow spectral bands in the visible and near-IR ranges at the same time.

The main problem with this technique is that four experimental points ($n = 4$) are not enough to determine two parameters ($p = 2$): temperature (T) and the emissivity (ε) that describe the Planck curve with the required accuracy [34]. The experimental statistical error or confidence contour for p parameters when fitted to n points using nonlinear regression is proportional to $p/(n-p)F(p,(n-p),(1-\alpha))$, where F is the Fisher distribution coefficient, and $(1-\alpha)$ is the value of the selected confidence probability [35]. The value of the statistical error sharply decreases with increasing difference $n-p$. In Campbell's four-wave system, $n-p=2$, which signifies that the statistical estimate of the temperature uncertainty is based on only two measurements, which severely limits the accuracy of temperature measurements. Another disadvantage of this system is the complexity of the alignment of the optical system, which consists of four cameras, in which it is necessary to achieve an exact match of the images with all the cameras. Apparently, due to the above reasons, this method has not been widely used in installations for laser heating in high-pressure cells [36, 37].

Systems based on mechanically switched spectral filters [38] that record images do not allow one to quickly obtain data, and a small number of recorded spectral points limits the accuracy of temperature determination. Kavner and Nugent proposed to combine a diffraction spectrometer and a video camera to measure the radial temperature profile in a laser-heated spot inside a cell [29, 39]. This method, called the 'peak scaling method,' consists in the fact that the temperature distribution is determined using two measurements. First, average temperature T_{av} of the heating region is measured using a diffraction spectrometer. Further, using the experimentally measured (linear) dependence of the temperature at the maximum T_{max} on T_{av}, one can obtain the temperature at the maximum heating T_{max}. Next, the heated region of the sample is photographed at a fixed wavelength. If we assume that the maximum intensity of the obtained monowavelength image corresponds to the temperature maximum T_{max}, then the temperature gradient on the sample surface can be obtained using Planck's law scaling. In this method, the temperature at each point of the surface is determined by only one measurement, which leads to a low measurement accuracy. In addition, the method described does not take into account the temperature dependence of the emissivity.

In 2016, a fundamentally new method was proposed for measuring the two-dimensional distribution of the surface temperature of a luminous body. The temperature distribution of a tungsten filament heated by direct current from a stabilized current source is determined using a double acousto-optic (AO) imaging filter [40]. Devices of this type are distinguished by their high spectral resolution, a fairly wide range of spectral tuning, arbitrary spectral addressing, high image quality, high speed, and the absence of moving elements [41]. Most important, in this method, the temperature at each point of a body heated by the laser is determined from a large set of experimental points on the Planck curve. This ensures a high accuracy of temperature measurement [42]. The purpose of this review is to present the latest results on the application of acousto-optic video spectrometry to study processes occurring at high pressures and temperatures.

2. Laser heating in high-pressure cells

High-pressure cells with diamond anvils are used to study a substance under conditions of high static pressures. Developed back in the late 1950s, the cells are unique experimental equipment for studying matter at high pressures [43, 44]. Samples placed in such cells usually have a diameter of 10–50 μm and a thickness of 5–20 μm in a pressure range up to 1 Mbar (Fig. 1). They are laid in a hole made in a specially prepared plate of steel or rhenium, called a gasquette. Prior to their placement, preliminary preparation is carried out. A recess is created in the gasquette by squeezing the diamonds. For pressures below 100 GPa, the thickness of the steel at the point of depression does not exceed 40 μm. Then, a hole with a diameter of about 100 μm is drilled inside the recess. This hole is the chamber where the sample is placed and where the sample is subjected to high pressures. Two small Al_2O_3 ruby samples are loaded into the chamber next to the sample. They are used as pressure sensors. The pressure can be determined from the shift of the ruby fluorescence line [45, 46]. The dimensions of the recess and hole depend on the pressure planned to be produced in the sample [47]. The pressure is created by squeezing the diamonds with three or four screws. The device with diamond anvils is capable of producing a working pressure of more than 600 GPa (6 Mbar) [9], which is one and a half times higher than the pressure at the center of Earth (3.6 Mbar). Diamond anvils weakly absorb electromagnetic radiation in a wide energy range, including the visible and IR regions of the spectrum, and are practically transparent to X-rays. These features make high-pressure cells with diamond anvils a unique tool for studying the mineral phases of Earth's deep interior, as well as for studying phase transitions in materials at high pressures [11].

To study the properties of minerals under conditions close to those in Earth's mantle or core, and to study phase

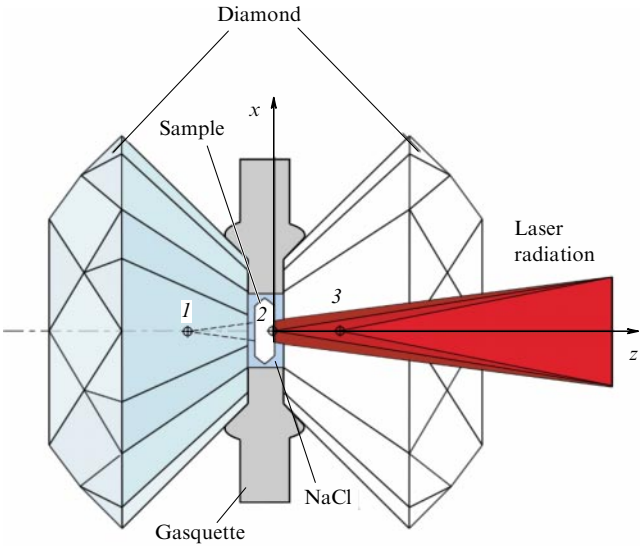

Figure 1. Schematic representation of laser heating in a high-pressure cell with diamond anvils; numbers *1*, *2*, *3* indicate the possible focusing points of laser radiation during heating. *1* — optimal focusing point, *2* — when focusing, heating area is minimal, heating is highly uneven, *3* — this option is dangerous, because the high energy density due to focusing inside the diamond anvil can damage it.

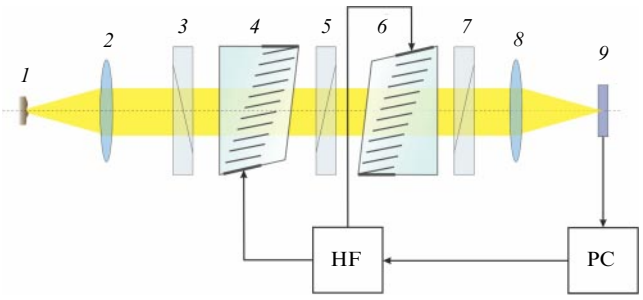

Figure 2. Double AO filter: *1* — object under study, *2* — microobjective, *3*, *5*, *7* — crossed polarizers, *4*, *6* — conjugated AO cells, *8* — objective, *9* — 2D array radiation detector, HF — high-frequency signal, PC — personal computer.

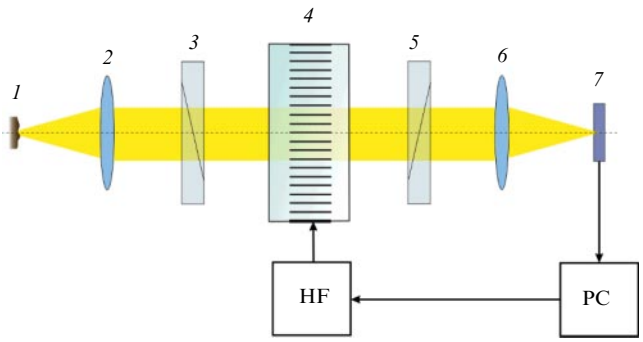

Figure 3. Setup for measuring the spatial distribution of the temperature of microobjects: *1* — object under study, *2* — microobjective, *3*, *5* — crossed polarizers, *4* — AO cell, *6* — objective, *7* — 2D array radiation detector, HF — high-frequency signal, PC — personal computer.

transitions in minerals and functional materials, the samples must also be at high temperatures. The sample is heated by a focused beam of an IR laser with a wavelength of 1.064 μm (Nd:YAG laser) with a power of 10–100 W (see Fig. 1). The sample temperature is measured, as a rule, by recording and analyzing the spectrum of thermal radiation emitted by the heated sample. Illumination of the sample and recording of thermal radiation are carried out through one of the two diamonds used for squeezing, which are transparent to laser radiation. Subsequent comparison of the measured spectrum and Planck's theoretical thermal radiation curve makes it possible to determine the temperature in the sample [48]. To reduce the temperature gradient inside the sample in installations operating, for example, on synchrotrons, heating is carried out from two sides [26]. The laser beam diameter on the sample surface does not exceed 25 μm [49].

3. Hyperspectral acousto-optic filtering for temperature determination using an acousto-optic filter

The Scientific and Technological Center of Unique Instrumentation (STC UI RAS) developed a new method and made a setup for measuring the spatial distribution of the surface temperature of samples at high pressures (up to 100 GPa) heated by a high-power laser (200 W). The main innovation of the developed method and setup is the use of a double tunable AO filter consisting of two conjugated AO crystals (*4* and *6*) assembled into a single system with a high-resolution video camera [40]. A schematic diagram of a double AO filter is shown in Fig. 2. The AO filter makes it possible to record images of a heated region at different wavelengths in a range of 650–1000 nm with an increment of 10 nm [41, 50]. Single tunable AO filters, as well as other spectral elements, have already been used for single-point temperature measurements [51, 52]. A detailed description of a portable AO-video spectrometer in which this approach is implemented can be found in Ref. [53].

The determination of the spatial temperature distribution $T(x, y)$ of an object is carried out by approximating the measured dependence $I(x, y, \lambda)$ of the Planck curve in each pixel using the least squares method [54]. The intensity of each point of the spectral image is proportional to the radiation intensity of the corresponding point of the heated body. A set of spectral images obtained in a range of 650–750 nm makes it possible to calculate the wavelength dependence of the radiation intensity of each point of the heated object. The distribution of temperature and emissivity of the surface of the heated body is obtained by fitting the experimental spectral dependence of the radiation intensity at each point of the heated object to the Planck distribution using the least squares method.

Each AO filter is a solid-state spectral bandpass filter operating on the principle of AO-anisotropic diffraction in a birefringent crystal [55, 56]. The AO filter usually consists of an AO cell and a pair of crossed polarizers (*3* and *5*) (Fig. 3). The AO filter is a TeO_2 crystal to which a piezoelectric transducer is attached. Attached to the opposite side of the crystal is an ultrasound absorber. In response to an oscillating RF electrical signal, the transducer generates a high frequency (HF) oscillatory (acoustic) wave that propagates through the crystal. Due to the elastic-optical effect, the propagating wave causes a change in the refractive index of the crystal with a period corresponding to the period of the propagating acoustic wave. For light propagating through a crystal, such a structure created by the acoustic wave is a moving bulk phase diffraction grating. Effective Bragg AO diffraction can take place only when the matching condition of light waves is satisfied [56].

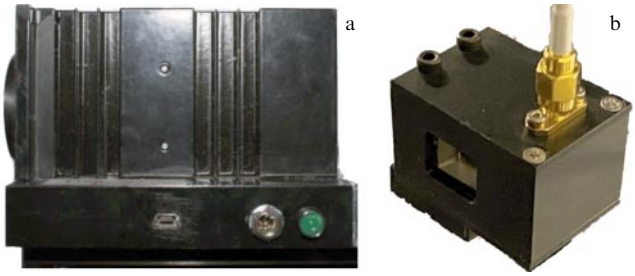

Figure 4. Photographs of acousto-optic filters: (a) double AO filter, device dimensions are 130 × 80 × 50 mm, inlet and outlet hole diameters are 8 mm, operating current is 0.7–1.1 A, supply voltage is 6 V; (b) single AO filter developed at the STC UI RAS.

Figure 5. Photograph of the setup for laser heating of substances in high-pressure cells.

The setup uses a double AO image filter consisting of two AO cells [41]. The AO filter was designed and assembled as a separate computer-controlled spectral imaging device (see Fig. 2). Its main parameters are: acoustic frequency range of 42–79 MHz; tuning range of 650–1100 nm; spectral resolution $\delta\lambda = 1.5$ nm (at $\lambda = 780$ nm); spatial resolution of 500 × 500 resolved elements; field of view of 3° × 3°; pupil entrance diameter of 8 mm; and residual spatial distortion of less than 0.1% of the field of view in the entire spectral range. Photographs of actually operating single and double AO filters developed at the STC UI RAS are shown in Fig. 4.

A photograph and diagram of the apparatus intended for laser heating in high-pressure cells are shown in Figs 5 and 6, respectively. The setup consists of a high-pressure cell mounting system with the possibility of remote motion of the sample during the laser heating experiment, an optical system for obtaining an image of the sample located inside the high-pressure cell, a powerful laser beam control system for heating the sample, and a system for measuring, during laser heating, the temperature distribution on a sample located inside the high-pressure cell (see Fig. 6).

The high-pressure cell is mounted on a three-axis motorized micrometer stage. The micrometer stage permits moving the sample in a range of 10–100 μm at 1.25 μm increments, which makes it possible to focus on the sample quite accurately. An ytterbium fiber laser with a wavelength of 1064 nm is used to heat the sample. On passing through a laser collimator, the laser radiation is incident on two mirrors (M_1 and M_2), which makes it possible to accurately control the beam in space and accurately introduce radiation into the π-Shaper lens.

The energy at the output of the laser collimator has a Gaussian distribution, but, after passing through the π-Shaper lens, the distribution of energy in the laser spot becomes more uniform. After the π-Shaper lens, a mirror (M_2) is installed, which reflects radiation with a wavelength of 1064 nm into a lens (O_1, ×20), with the sample at its focus. The sample is heated by the IR radiation. The radiation emanating from the sample is collected by the same lens (O_1, ×20) and enters an acousto-optical filter (AOF). The radiation passed through the monochromator (AOF) is focused by the lens (L_1) onto a 2D array radiation detector (ARD) of the video camera. The laser radiation is rejected with high efficiency by a special narrow-band filter ($M_{\lambda=1064}$). To increase the intensity of the optical signal, the illuminated optical branches are turned off during experiments by shifting the beam splitters (BS_1, BS_2). To control the pressure in the chamber of the high-pressure cell, a laser with a wavelength of 532 nm is installed in the setup. The laser radiation is focused on a pressure indicator: a spherical ruby particle 1–3 μm in diameter. The fluorescence of the spherical ruby particle is recorded by a spectrometer, and the pressure in the cell is calculated from the resultant data on the position of the ruby fluorescence peak.

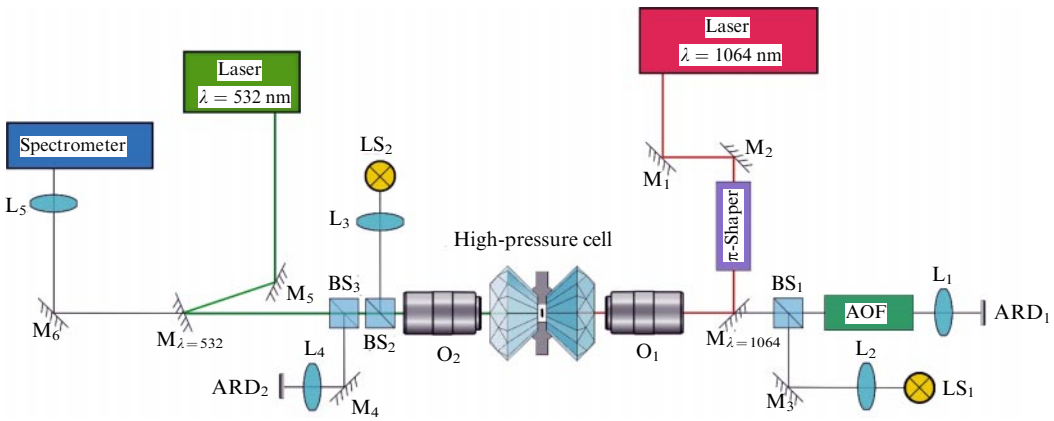

Figure 6. Schematic representation of the setup for laser heating in high-pressure cells (see explanations in the text).

4. Temperature determination by the least squares method based on Planck's law

The narrow wavelength range used in this work (740–800 nm) makes it possible to work within the framework of the 'gray body' radiation model, which implies that the thermal emission coefficient is independent of its wavelength [57]. Traditionally, the calculation of temperatures and thermal emissivity is carried out by comparing the data of spectral measurements with the Planck curve. Within the framework of the gray body model, Planck's law is of the form [58]

$$I(\lambda, T) = \varepsilon g(T, \lambda), \quad g(T, \lambda) = \frac{c_1}{\lambda^5 \left[\exp(c_2/\lambda T) - 1\right]}, \qquad (1)$$

where $I(\lambda, T)$ is the spectral intensity, ε is the thermal radiation coefficient of the heated object, λ is the wavelength, T is the temperature, and c_1 and c_2 are physical constants.

Digital processing of spectral images of the samples under study consists of measuring the intensity of spectral radiation in each pixel of multispectral images with subsequent determination of the temperature and thermal emission coefficient by the least squares method [59]. The optical system was calibrated using images of a certified tungsten incandescent lamp at a temperature of 1700 K [34]. The radiometric power supply provided very accurate and reproducible lamp current and constant radiation. A lamp with a known temperature was placed at the focus of the optical system in the position usually occupied by the sample.

The method for determining the temperature from experimental data for $I(\lambda)$ is to find such values T_0 and ε_0 at which the sum of the squared deviations of the experimental intensity values $I(\lambda_i)$ from the corresponding theoretical values,

$$S(\varepsilon, T) = \sum_{i=1}^{N} \left[I(\lambda_i) - \varepsilon g(\lambda_i, T)\right]^2, \qquad (2)$$

has a minimum (two-dimensional nonlinear minimization). In expression (2), N is the number of measurements. Calculations based on experimental data have shown that the search for the global minimum of the function $S(T, \varepsilon)$ requires a significant amount of computer time and strongly depends on the correct choice of initial values of parameters ε_0 and T_0. Specifically, the use of two-dimensional nonlinear minimization (2) to find ε_0 and T_0, as well as the calculation of the spatial distribution of the sample temperature in the heating region, can take several hours. It should be noted that, for temperatures below 4000 K, $\lambda T \ll c_2$, advantage is often taken of the Wien approximation

$$I(\lambda, \varepsilon, T) = \frac{\varepsilon c_1}{\lambda^5 \exp(c_2/\lambda T)}. \qquad (3)$$

Using this approximation and moving to logarithmic coordinates, one can obtain the spectral distribution in the form

$$J = \ln\left(\frac{I(\lambda)\lambda^5}{c_1}\right) = \ln\varepsilon - \frac{c_2}{\lambda T}. \qquad (4)$$

The resultant linear dependence makes it possible to separately determine the temperature and the spectral emissivity. In Wien's coordinates, the temperature will be inversely proportional to the slope of the straight line (4), and the intersection of the y-axis is determined by the emissivity.

Using the Wien approximation to determine the temperature and emissivity has two drawbacks. First, as was shown in Ref. [60], with increasing temperature, the error associated with the use of approximation (4) increases as T^2. In order to show this, we introduce new variables into equation (4):

$$J_i = a + \tau x_i, \quad a = \ln\varepsilon, \quad x_i = \frac{c_2}{\lambda_i}, \quad \tau = -\frac{1}{T}. \qquad (5)$$

Then, equation (2) can be written as

$$S(\varepsilon, T) = \sum_{i=1}^{N} \left[J(\lambda_i) - a - x_i\tau\right]^2. \qquad (6)$$

For a linear regression, statistical errors for regression coefficients can be written in an analytical form [61]:

$$\sigma_a = \sigma_y \sqrt{\frac{\sum x_i^2}{N\left(\sum x_i^2\right) - \left(\sum x_i\right)^2}},$$

$$\sigma_\tau = \sigma_y \sqrt{\frac{N}{N\left(\sum x_i^2\right) - \left(\sum x_i\right)^2}}, \qquad (7)$$

where

$$\sigma_y = \sqrt{\frac{\sum_{i=1}^{N}(J_i - a - \tau x_i)^2}{N-2}}, \qquad (8)$$

σ_a is the standard deviation of parameter a in the equation, and σ_τ is the standard deviation of parameter τ. To obtain expressions for the standard deviations ε and T, one can use the formula that relates the standard deviations of direct and indirect measurements:

$$\sigma_\varepsilon = \varepsilon\sigma_a, \qquad (9)$$

$$\sigma_T = T^2\sigma_\tau. \qquad (10)$$

Moreover, as can be seen from formula (10), the temperature measurement error in the Wien approximation is proportional to T^2. Therefore, to correctly estimate the temperature and emissivity, it is necessary to use the least squares method using formula (2), i.e., to minimize the function S in two parameters, which significantly increases the time for calculating the temperature on a computer (up to 1 hour). To reduce the calculation time for ε_0 and T_0, a new procedure was proposed for finding the minimum of function (2) using the least squares method [62]. It is based on the fact that the thermal radiation coefficient ε in expression (1) is a linear parameter. As follows from the theorem on the necessary condition for the existence of an extremum of a continuous function, $S(T, \varepsilon)$ has a minimum for such values of T_0 and ε_0, whereby the following conditions are satisfied: $\partial S/\partial T|_{T=T_0, \varepsilon=\varepsilon_0} = 0$, $\partial S/\partial\varepsilon|_{T=T_0, \varepsilon=\varepsilon_0} = 0$ [62]. Solving the first equation gives the value of ε at the minimum at a given temperature:

$$\varepsilon = \frac{\sum_{i=1}^{N}\left[I(\lambda_i)\, g(\lambda_i, T)\right]}{\sum_{i=1}^{N}\left[g^2(\lambda_i, T)\right]}. \qquad (11)$$

Equation (11) can be used to get the T_0 value. Specifically, we substitute expression (11) into Eqn (2) to obtain

$$S(T) = \sum_{1}^{N}\left[I(\lambda_i) - \frac{\sum_{i=1}^{N}\left[I(\lambda_i)\, g(\lambda_i, T)\right]}{\sum_{i=1}^{N}\left[g^2(\lambda_i, T)\right]} g(\lambda_i, T)\right]^2. \qquad (12)$$

It can be seen that the function $S(T)$ in expression (12) depends on only one parameter, the temperature. Therefore, the described procedure reduces the two-dimensional nonlinear minimization of function (2) to a one-dimensional search for the minimum of function (12). This leads to a multiple reduction in the temperature calculation time, which is especially important for studying the temperature distribution of a surface heated by a laser, as well as for correctly calculating the experimental error [60].

When expression (12) is used to find the temperature and emissivity, one can also obtain an analytical expression for the RMS standard deviation for the emissivity [34]. Consider Eqn (11) at points T_0 and ε_0. If it is assumed that all measurements $I(\lambda_i)$ are independent, then the standard deviation of the emissivity can be written as

$$\sigma_\varepsilon^2 = \sum_{i=1}^{N} \left[\frac{\partial \varepsilon(\lambda_i)}{\partial I} \sigma_I \right]^2 , \tag{13}$$

where

$$\sigma_I = \sqrt{\frac{\sum_{i=1}^{N} \left[I(\lambda_i) - \varepsilon_0 g(\lambda_i, T_0) \right]^2}{N-2}} .$$

The partial derivative in Eqn (13) can be obtained in an analytical form:

$$\frac{\partial \varepsilon(\lambda_i)}{\partial I} = \frac{g(\lambda_i, T)}{\sum_{i=1}^{N} \left[g^2(\lambda_i, T) \right]} .$$

Then, the expression for the standard deviation ε can be written as

$$\sigma_\varepsilon = \frac{\sigma_I}{\sum_{i=1}^{N} \left[g^2(\lambda_i, T_0) \right]} . \tag{14}$$

The temperature measurement error for a given confidence level can only be obtained numerically [34]. Interestingly, we have not been able to find analytical expressions similar to Eqns (9), (10), and (14) in scientific publications, despite the long history of temperature measurements using Planck's law or Wien's approximation.

5. Hyperspectral imaging for measuring the temperature distribution of materials at high temperatures and pressures

Experiments using a double AO filter showed the effectiveness of this method for measuring the temperature distribution on the surface of samples during laser heating both at normal [40, 63, 64] and high pressures [34, 60, 65, 66]. Figure 7 shows the temperature distribution on the surface of boron carbide (BC) at a pressure of 24 GPa heated by a high-power laser in a high-pressure cell. The number of spectral images obtained with the AO filter was $N = 61$ at 2 nm increments over the spectrum in the tuning range from 620 to 750 nm. The highest temperature in the heating region was 2452 K and the lowest was 1190 K.

In Ref. [34], the values of statistical errors of temperature measurements were compared between the methods using an AO filter and the four-color method (Fig. 8). This can be done by selecting thermal radiation measurements at only four wavelengths ($n = 4$) out of the 78 measurements typically made during AO filter measurements. It was shown that, at a

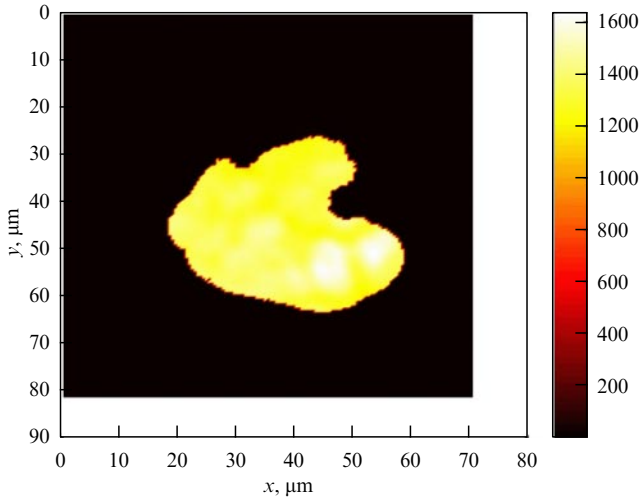

Figure 7. (Color online.) Temperature distribution on BC surface during heating in a high-pressure cell at a pressure of 24 GPa. Laser power: 30 W; wavelength range: 620–750 nm, exposure time: 2 s.

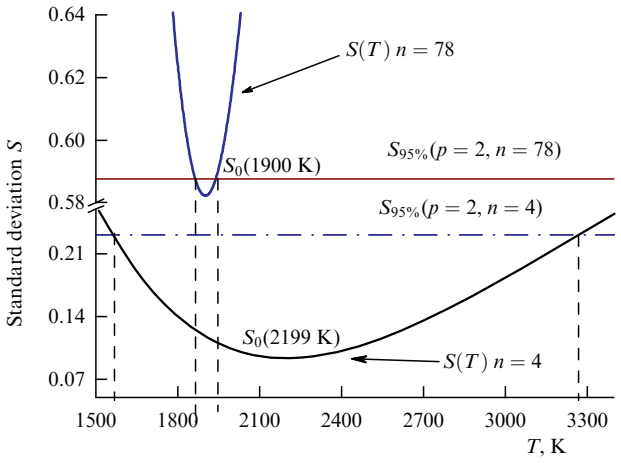

Figure 8. Fitting of experimental data using the 1D minimization procedure to determine the temperature of a tungsten lamp at electric current $i = 11.25$ A with a different number of experimental points n. For $n = 78$, the sum of squared deviations $S(T)$ has a minimum at 1900 K (95% confidence interval is 1900 ± 38 K), for $n = 4$ the value of $S(T)$ has a minimum at 2199 K (95% confidence interval is 2199 ± 850 K) [34].

95% confidence level, the confidence interval was $\Delta T = \pm 38$ K. Measurements at only four points gave the following value of the confidence interval: $\Delta T = \pm 850$ K, which is 20 times worse than the value of the interval obtained for $n = 78$. On this basis, it can be concluded that the four-color method does not provide the necessary accuracy of temperature distribution measurements [67].

6. Use of a one-crystal acousto-optic filter to measure the temperature distribution of a heated body

The use of a double AO filter to measure the temperature distribution during laser heating was due to the high efficiency of such filters in compensating the chromatic drift of the AO spectroscopic image in an imaging system with an AO filter [34]. Unfortunately, the time exposure of the double AO filter is not short enough to perform dynamic measure-

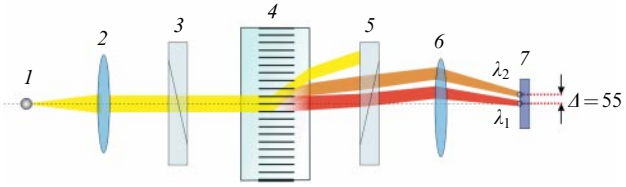

Figure 9. Transverse chromatic aberration ($\Delta = 55$ pixels) in a single tunable AO filter and in images at $\lambda_1 = 640$ nm and $\lambda_2 = 740$ nm: *1* — test object, *2* — lens, *3* and *5* — crossed polarizers, *4* — tunable AO filter, *6* — lens, *7* — camera with a Sony CMOS Pregius array sensor (pixel size of 3.45 × 3.45 μm) [67].

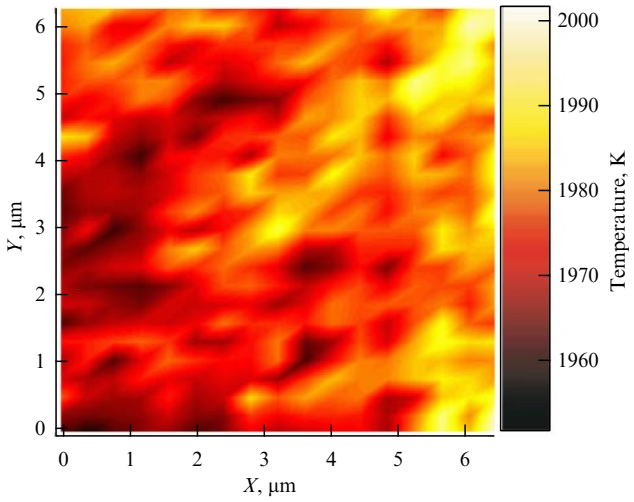

Figure 10. (Color online.) Temperature distribution on the surface of a lamp heated by a current of 10 A.

ments of the temperature distribution at times shorter than 0.3 s. This makes it impossible to measure temperatures below 1000 K. To reduce the exposure time, a setup was made and the first measurements were made using a single AO filter [63]. It was shown that the use of a single AO filter leads to a twofold increase in the intensity of multispectral images compared to a double AO filter. The strong chromatic drift of the AO spectroscopic imaging system was compensated by using the developed software, which makes it possible to align all images recorded at different wavelengths. As a result, the threshold for measuring the minimum temperature becomes lower and the exposure time also shortens, which makes it possible to increase the speed of capturing hyperspectral images by several times.

The main problem with using a single AO filter for visualization is the presence of transverse chromatic aberrations, which lead to a transverse shift of the image in the diffraction plane (Fig. 9). To reduce the effect of transverse chromatic aberrations in the manufacture of an AO filter, the input and output faces of the crystal are cut at certain angles. In order to reduce reflection losses, the input face is cut so that it is orthogonal to the incident beam. The output face of the filter is cut at an angle.

To compare the results obtained using double and single AO filters, experiments were performed with the heating of a tungsten lamp. A lamp with a uniformly heated flat tungsten ribbon was used as a radiating heated object. The lamp temperature was determined by fitting the actual signal to Planck's equation at each point on the sample surface (Fig. 10). Since the temperature of a heated body must be uniformly distributed over the surface of such a test object, the recorded temperature changes (~ 60 K) over the surface are associated with the error of the methods implemented with tunable AO filters.

Note also that the confidence interval when using a single AO filter is 30% smaller than in the case of a double one. This may be due to the fact that the exposure time for the single AO filter is a little more than one third of that when using the double filter.

It has been experimentally determined that the transmittance of a single AO filter is 2.8 times higher than that of a double one, allowing us to reduce the exposure time of the camera's array radiation detector when shooting a series of images and, as a result, speed up data collection. It was shown that the use of a single AO filter together with the AO-image correction algorithm makes it possible to measure the temperature of heated objects.

7. Measurement of the distribution of the thermal radiation coefficient of materials

The coefficient of thermal radiation of materials is one of the fundamental properties of thermal radiation. It represents the ratio of the intensity (or brightness) of the body's radiation to the corresponding value for a black body in a given direction. Measurement of the directional thermal radiation coefficient at high temperatures is important for understanding many physical phenomena, such as the transfer of thermal radiation in Earth's core [68], processes in a diffusion flame [68], the production of solar cells with a low thermal radiation coefficient [69], thermal spacecraft control, and highly efficient use of solar energy.

The current state of the methods for determining the thermal radiation coefficient can be found in Ref. [69]. Direct radiometric methods are based on comparing the surface thermal radiation of the materials being studied with a calibration object (black body) under the same temperature, geometric, and spectral conditions [69]. The choice of heating method depends on the material of the object under study (electrical and thermal conductivity) and on the measured temperature range. High temperatures (> 2000 K) can be obtained by heating with laser radiation [70–72]. One of the most popular methods for measuring the temperature during laser heating is the two-color method [73]. Its modification, the four-color method, was used to measure the temperature distribution in high-pressure cells in samples heated by high-power laser radiation and was described in Ref. [33]. Unfortunately, the use of the four-color method to study the distribution of the thermal emissivity in the region of heating at high pressures did not meet with success: the authors managed to determine only the change in the value of the thermal emissivity for platinum as a function of temperature, and not the absolute values of this quantity [36]. One of the main disadvantages of the four-color method is the small number of points (four) for finding two parameters (temperature and thermal emissivity) from the data on measuring the thermal radiation of a heated sample.

The possibility of using the multispectral imaging method to measure the distributions of the thermal emissivity together with the temperature distribution in samples heated by laser radiation was demonstrated in [60]. A tungsten lamp was chosen as a test sample in this study. This choice is due to the fact that tungsten is one of the most widely used high-

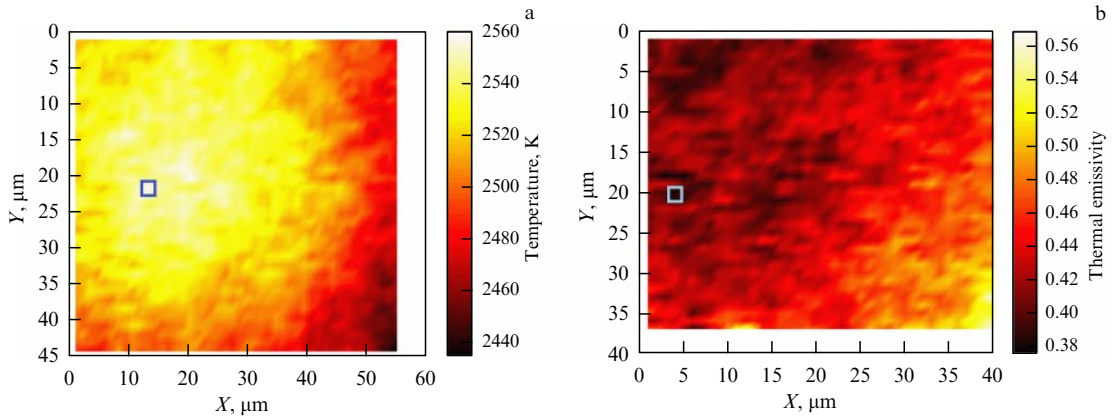

Figure 11. (Color online.) Temperature (a) and thermal emissivity (b) distributions in the heating of a tungsten lamp by 8-W laser radiation; exposure time is 0.25 s. Number of multispectral images obtained with a double AO filter was $N = 61$ at increments of 1 nm in the spectral range from 740 to 800 nm (constructed based on data presented in Ref. [60].

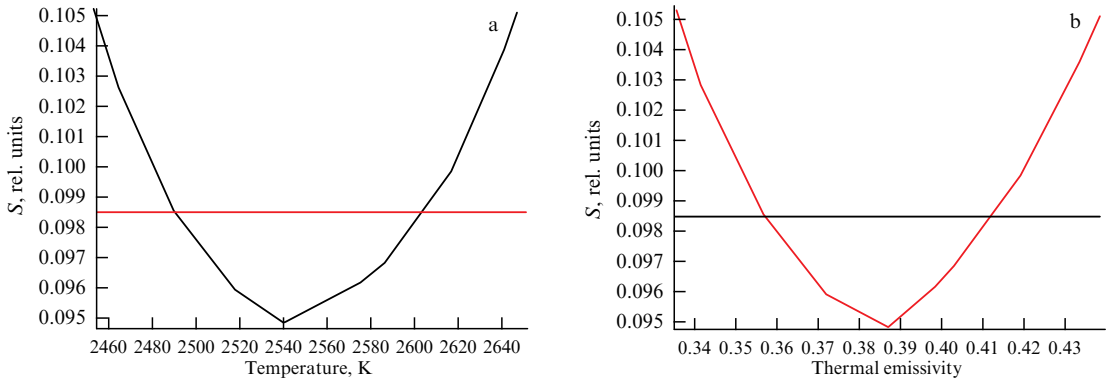

Figure 12. Behavior of the sum of squared deviations S as a function of temperature (a) and thermal radiation coefficient (b) at a selected point at the center of the heating spot. Intersections of the horizontal line with function S determine the confidence interval within which the temperature values lie with a confidence probability of 0.95. Calculation of the confidence region, in this case the level of the horizontal line, using the Fisher criterion is described in Ref. [34] (plotted on the basis of data presented in Ref. [60]).

temperature materials [54]. It is well studied and, what is very valuable, there is a database of tabular data for the emissivity at various temperatures and wavelength ranges.

During the experiment, a laser beam with a power of 8 W was focused on a tungsten plate inside a vacuum lamp. Figure 11 shows the resultant distributions for the temperature (Fig. 11a) and thermal radiation coefficient (Fig. 11b). The highest temperature in the heated section under investigation was 2540 K, and the lowest temperature was 2380 K. The size of the laser-heated area being studied was 45×60 μm. The value of the thermal radiation coefficient at the point of maximum heating (2540 K) was 0.387. With a change in the measured temperature from 2380 to 2540 K (a scatter of 160 K), the thermal radiation coefficient varied from 0.38 to 0.56 (a scatter of 0.18).

The behavior of the sum of squared deviations of the experimental data from the theoretical ones as a function of temperature and emissivity at the maximum temperature point is shown in Figs 12a and 12b, respectively. With a confidence level of 0.95, the temperature confidence interval was ±55 K (2.2%), while the relative uncertainty for the emissivity is more than three times higher at ±0.027 (7%).

At the same time, the data suggest that a large temperature difference in the heating region under study introduces a serious error in the measurements of the emissivity at the edges of the spot. Specifically, an uncertainty of 7% for the maximum temperature of a heating spot of 2540 K ($\varepsilon_{ref} = 0.387$, $\varepsilon_{exp} = 0.398$) increases more than three times at the edges of the spot, where the temperature is 2380 K ($\varepsilon_{ref} = 0.403$, $\varepsilon_{exp} = 0.55$). The notation used here: ε_{ref} — reference data, ε_{exp} — experimental data.

The method described in the paper, in combination with a laser heating system, made it possible for the first time to obtain the distribution of the thermal emissivity along with the temperature distribution. This was made possible by point-by-point measurement of parameters over the entire area under study.

8. Two-dimensional distribution of laser beam intensity on a sample surface

The measurement of the temperature distribution over the surface of a sample heated by laser radiation is highly sensitive to the position of the focal plane of the laser beam. Due to the fact that IR-laser radiation at a wavelength of 1064 nm cannot be observed visually, since it lies outside the visible range, finding the focal plane of the IR-laser radiation is not an easy task. It turns out that the use of a double AO filter makes it possible to visualize the IR-laser intensity distribution on the surface of a heated sample [66]. The dual AO filter is tuned to a wavelength of 1038 nm. This makes it possible, first, to visualize the radiation of the IR laser on the camera and, second, to determine the position of the focal plane of the IR laser. Assuming that the resultant values of laser intensity

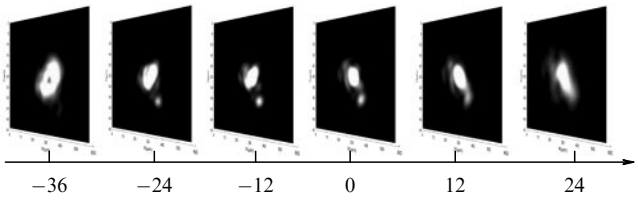

Figure 13. Images of an IR laser beam taken at a wavelength of 1038 nm at different defocusing values (Z positions). The position $Z = 0$ corresponds to the focusing of a 5-W IR-laser on the sample surface [66].

at 1038 nm are proportional to the laser intensity at 1064 nm, the image measured on the double AO filter at 1038 nm represents the shape of the laser intensity distribution on the surface of the heated object.

Figure 13 shows the IR-laser radiation distributions measured near the focal plane of the reflective plate. The diameter of the laser spot at the focus is about 8 μm, and the actual depth of focus is 96 μm. As shown in Ref. [766, the use of a double AO filter to visualize IR-laser radiation is a powerful tool not only for adjusting the IR laser but also for controlling the distribution of the IR-laser power on the sample surface during heating. In the future, we plan to use this method to conduct experiments to measure the thermal conductivity of materials at high pressures, as well as to observe the melting of materials under conditions of high pressures and temperatures.

Figure 14 shows the intensity and temperature distributions on the surface of a Pt plate placed in a high-pressure cell and heated by a laser. The size of the region with a temperature above 1700 K is very close to the size of the laser spot. The apparent size of the focal spot is 5 μm; the real size is 7% smaller for a diamond with a diameter of 2.5 mm [32].

9. Determination of the melting point of solids using an imaging acousto-optic filter

Laser heating in high-pressure cells with diamond anvils plays an important role in studying the physical and chemical properties of different materials, including minerals under conditions corresponding to those inside Earth [26]. In experiments on laser heating, the melting point of a solid body cannot always be determined by contact techniques. To determine the melting temperature during laser heating of materials under high pressure conditions, various detection techniques can be used: direct visual observation of motion during melting, a change in the reflectivity of the sample, discontinuity in the dependence of laser power on temperature, changes associated with melting on the surface of the sample, and vanishing of X-ray diffraction lines [74, 75]. However, many seemingly simple material studies have caused controversy due to disagreements and differences both among the results of different experiments and between experimental and theoretical data [80]. Unfortunately, all of these techniques have significant drawbacks. For example, the use of X-ray diffraction is impossible for amorphous materials. But the main disadvantage of these techniques is the nonuniformity of the temperature distribution on the surface of laser-heated materials.

In Ref. [49], a new method was proposed for determining the melting temperature of a solid under laser heating. In order to detect the onset of melting, we analyze speckle interference patterns on a selected area of a solid sample surface heated by a laser. Analysis of speckle interference patterns in a laser-heated system has already been used to quantitatively measure the melting onset temperature [76, 77]. Unfortunately, no quantitative criteria for determining the melting point have been proposed. The advantage of our approach is that our developed laser heating system equipped with a double AO filter makes it possible to determine the temperature distributions [34]. For this reason, the procedure for measuring the melting temperature is more accurate than using a diffraction spectrometer or any other spectral equipment that measures the temperature averaged over the heating area.

A study was made of the behavior of the speckle pattern as a function of temperature during laser heating of the surface of a tungsten plate in a vacuum spectral lamp (SI6-100, Russia). It was found that the image at a frequency of 1040 nm had a speckle structure when the roughness of the surface sample was sufficiently high. Figure 14 shows the temperature distribution over a plate heated by a high-power laser (9 W), and shown in Fig. 15 is the image of a laser-illuminated region taken at a wavelength of 1038 nm and showing a pronounced speckle pattern. Image analysis suggests that the dynamics of the speckles depends on the laser intensity. Since the temperature of the laser-heated sample is nonuniform (see Fig. 15), the dynamics of the speckle fluctuations must also be nonuniform (Fig. 16). To study this issue, we analyzed the dynamics of speckle fluctuations during laser heating in the region where the intensity of fluctuations turned out to be highest. Selected for analysis was the area inside the rectangle S, shown in Fig. 16.

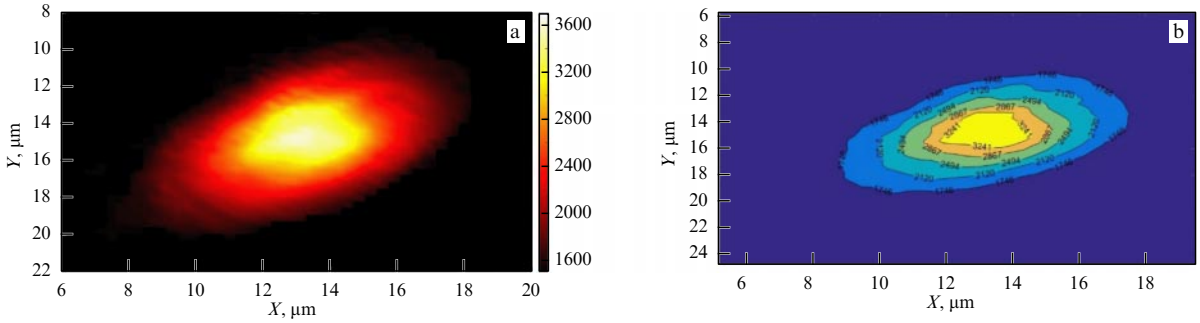

Figure 14. (Color online.) (a) Intensity distribution of an IR laser beam on the surface of a Pt plate heated in a high-pressure cell at 40 GPa and a laser power of 16 W. (b) Temperature distribution measured with a double AO filter in the wavelength range of 640–750 nm with an exposure time of 6 s. The contour plot displays the contour lines of the color map with filled areas between the contour lines.

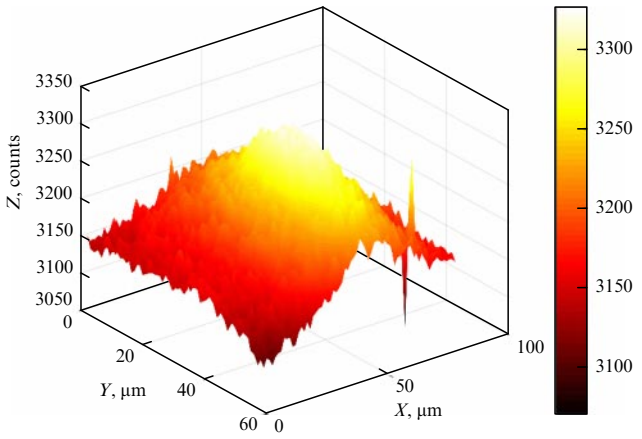

Figure 15. (Color online.) Temperature distribution on the surface of a tungsten plate at an IR laser power $P = 9$ W. Exposure time: 1 s. Plotted on the basis of data presented in Ref. [78].

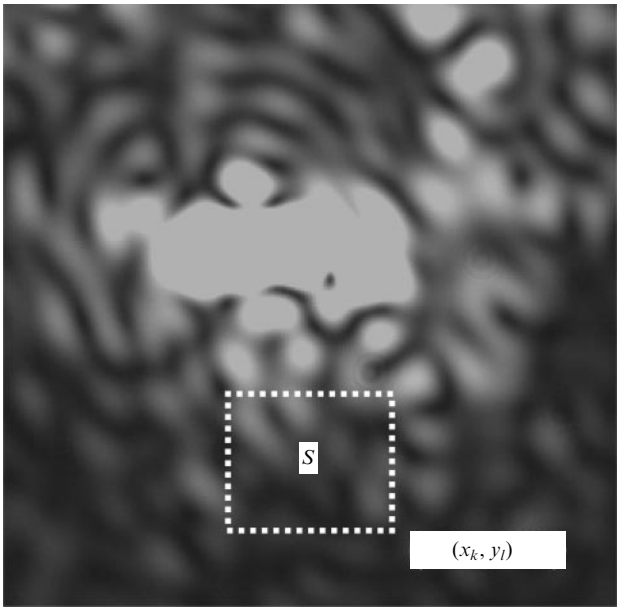

Figure 16. Speckle image of reflected IR laser radiation obtained at a filter wavelength of 1040 nm. Exposure time: 1 ms; field of view: 127 × 163 μm. The analyzed area is marked with a rectangle. Plotted on the basis of data presented in Ref. [78].

We denote the coordinate of each pixel in the selected area S as (x_k, y_l), where the indices k and l vary in the range $k = 1 \ldots K$, $K = 65$, $l = 1 \ldots L$, $L = 58$. Let $I(P, t_i, x_k, y_l)$ be the intensity of IR radiation at a wavelength of 1040 nm reflected from a pixel with coordinates (x_k, y_l) at the point in time t_i, and P be the radiation power of the IR laser. When performing laser heating, $I(P, t_i, x_k, y_l)$ is written at intervals Δt, so that $t_i = t_0 + i\Delta t$, where $i = 1, 2, 3, \ldots, N$.

The absolute value of the difference between the intensities at the point in time t_{i+1} and the current time t_i in a pixel (x_k, y_l) will be denoted as $\Delta I(P, t_i, x_k, y_l)$:

$$\Delta I(P, t_i, x_k, y_l) = \left| I(P, t_{i+1}, x_k, y_l) - I(P, t_i, x_k, y_l) \right| . \qquad (15)$$

Figure 17 serves to illustrate the behavior of $\Delta I(P, t_i, x_k, y_l)$ as a function of time with increments $\Delta t = 1$ s. One can see that during heating for 4 s the nature of the speckles changes significantly. To obtain a numerical

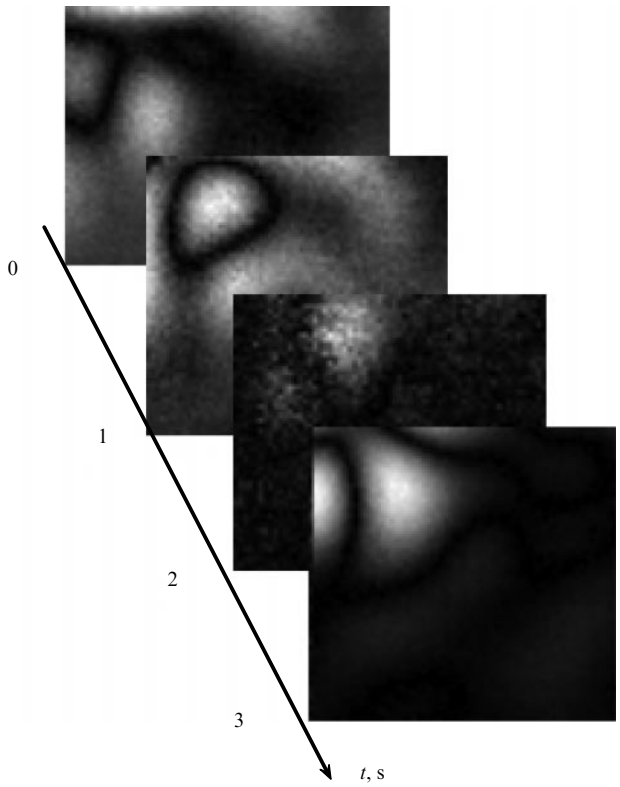

Figure 17. Speckle image of the sample's selected area S with intervals of 1 s. The wavelength of the acousto-optical filter is 1040 nm, the laser power is 12 W. Plotted on the basis of the data presented in Ref. [78].

estimate of fluctuations in the speckle intensity, ΔI, during laser heating, we introduce the average value $\Delta I(P, t_i, x_k, y_l)$ inside the selected region S at the point in time t_i, $\Delta I_S(P, t_i)$:

$$\Delta I_S(P, t_i) = \frac{\sum_{k=1}^{k=K} \sum_{l=1}^{l=L} \Delta I_S(P, t_i, x_k, y_l)}{KL} . \qquad (16)$$

We denote the average value of $\Delta I_S(P, t_i)$ during laser heating as $\langle \Delta I_S(P) \rangle$:

$$\langle \Delta I_S(P) \rangle = \frac{\sum_{i=1}^{i=N} (P, t_i)}{N} . \qquad (17)$$

Then, the speckle intensity fluctuation at the point in time t_i can be characterized by the parameter $\delta(P, t_i)$,

$$\delta(P, t_i) = \Delta I_S(P, t_i) - \langle \Delta I_S(P) \rangle . \qquad (18)$$

The temporal behavior of the fluctuation $\delta(P, t_i)$ measured for two laser powers P is shown in Fig. 18. One can see that the behavior of $\delta(P, t_i)$ has a pronounced oscillatory character and that, the higher the intensity of the heating laser, the higher the amplitude of the oscillations. Since the fluctuations have different signs, we introduce a quantity similar to the variance in statistics, namely the average squared fluctuation value $\delta^2(P)$:

$$\delta^2(P) = \frac{\sum_{i=1}^{i=N} \delta^2(P, t_i)}{N - 1} . \qquad (19)$$

The variance of fluctuations $\delta^2(P)$ of the radiation intensity reflected from the selected area as a function of temperature is shown in Fig. 19. It can be seen that the

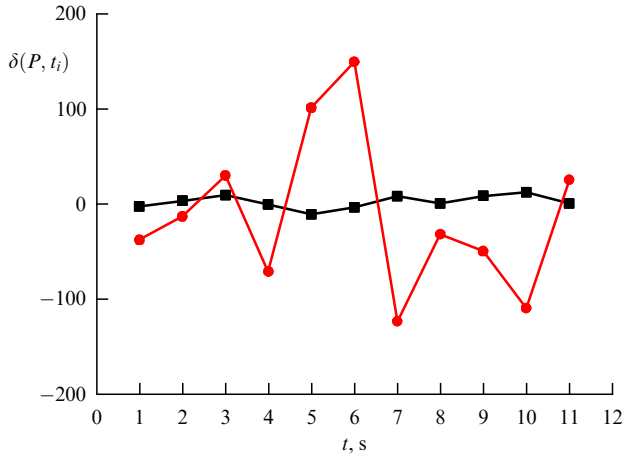

Figure 18. Behavior of parameter $\delta(P, t_i)$ as a function of time for different values of IR-laser power [78].

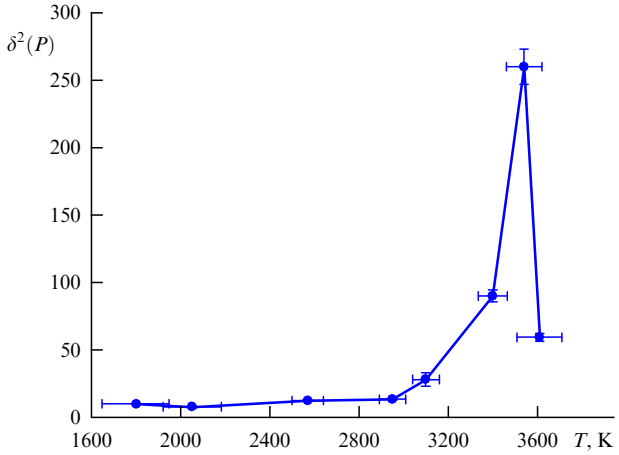

Figure 19. Variance of fluctuations $\delta^2(P)$ inside selected region S as a function of temperature [78].

fluctuation variance increases with the power of the heating laser. The variance peaks at a power of 13 W. This behavior during heating is explained by the melting of tungsten: as the power increases above 13 W, liquid tungsten flows out of the laser spot.

The proposed technique exhibits two main advantages over other methods. First of all, it allows us to study the dynamics of melting: we can determine the starting point of melting (3000 K in Fig. 19) and the point at which the solid body melts (3540 K in Fig. 19). All known techniques make it possible to determine the melting point. Furthermore, it is possible to study the temperature dependence of the melting in the same area, since a strong temperature gradient is observed at the site of laser heating. The possibility of studying the speckle dynamics of a small selected field in a heated region has an advantage over the technique proposed in Ref. [77], where the correlation method is applied to the entire heated region during laser heating. As a result, the variation in the correlation function is not as sharp as that in the speckle intensity fluctuation (19) near the melting point, which makes it difficult to determine the temperature very accurately.

So, it was shown in Ref. [49] that the use of a double AO filter and an analysis of the dynamics of speckle patterns makes it possible to determine the melting temperature of a tungsten plate and, therefore, makes it possible to study the melting of tungsten during laser heating. A sharp change in speckle fluctuations is especially noticeable when the temperature approaches the melting point. The speckle variance peak occurs at the temperature when the melting point is reached.

10. Conclusions

It was demonstrated that the combination of a laser heating system in high-pressure cells (LH-DAC) and a double acousto-optic filter (TAOF) allows one to simultaneously control the relative power distribution of an IR laser (1070 nm) on the surface of a sample placed in a high-pressure cell (DAC) and to measure the temperature distribution during laser heating of the sample under high pressure in the DAC. It is shown that the temperature distribution at high pressures and strong heating can be measured with an accuracy of 2% using the LH-DAC-TAOF method. The lower limit of temperature measurement for the method under description with the same data acquisition time is limited by the sensitivity of the AO filter in use and is estimated at 1000 K. The efficiency of the method was demonstrated in problems where it is necessary to measure the emissivity distribution under conditions of uneven high-temperature heating by laser radiation.

The use of LH-DAC-TAOF made it possible to develop a remote method for monitoring the melting point of the substances studied in DACs based on speckle interferometry; develop a method for measuring the static thermal conductivity of materials at high pressures and temperatures based on the simultaneous control of the intensity profile of laser radiation and the temperature distribution profile on the surface of a heated substance; and carry out experiments to measure the temperature distribution and emissivity of materials at pressures of 43 and 55 GPa and heated by high-power laser radiation.

Acknowledgements. This study was supported by the Russian Foundation for Basic Research under grant no. 20-18-50322. The experimental part was performed using the equipment of the unique scientific installation Laser Heating in High-Pressure Cells of the Scientific and Technological Center of Unique Instrumentation of the Russian Academy of Sciences [http://ckp-rf.ru/usu/507563/].

References

1. Bridgman P W *The Physics of High Pressure* (London: G. Bells and Sons, 1931); Translated into Russian: *Fizika Vysokikh Davlenii* (Moscow: ONTI, 1935)
2. Stishov S M *Azbuka Vysokikh Davlenii* (ABC of High Pressures) (Moscow: Inst. Komp'yut. Issled., 2019)
3. Boldyreva E V et al. *Issledovanie Tverdofaznykh Prevrashchenii pri Pomoshchi Rentgenovskoi Difraktsii v Usloviyakh Vysokikh Davlenii in situ* (Solid-Phase Transformations Research by X-Ray Diffraction under High-Pressure Conditions in situ) (Novosibirsk: Izd. SO RAN, 2016)
4. Popova S V, Brazhkin V V, Dyuzheva T I *Phys. Usp.* **51** 1064 (2008); *Usp. Fiz. Nauk* **178** 1104 (2008)
5. Savvatimskii A I, Onufriev S V *Phys. Usp.* **63** 1015 (2020); *Usp. Fiz. Nauk* **190** 1085 (2020)
6. Anderson D L *Theory of the Earth* (Boston: Blackwells Scientific Publ., 1989)
7. Hemley R J, Bell P M, Mao H K *Science* **237** 605 (1987)
8. Boehler R, Chopelas A *Geophys. Res. Lett.* **18** 1147 (1991)
9. Dubrovinsky L et al. *Nat. Commun.* **3** 7 (2012)

10. Tateno S et al. *Science* **330** 359 (2010)
11. Bassett W A *High Pressure Res.* **29** (2) CP5-186 (2009)
12. Murakami M et al. *Geophys. Res. Lett.* **32** 4 (2005)
13. Eremets M I et al. *Nat. Mater.* **3** 558 (2004)
14. Zinin P V et al. *J. Appl. Phys.* **111** 114905 (2012)
15. McMillan P F *Nat. Mater.* **1** (1) 19 (2002)
16. Riedel R et al. "Superhard materials", in *Handbook of Solid State Chemistry* (Eds R Dronskowski, Sh Kikkawa, A Stein) (Weinheim: Wiley-VCH, 2017) p. 175
17. Brazhkin V V *Phys. Usp.* **63** 523 (2020); *Usp. Fiz. Nauk* **190** 561 (2020)
18. Dubrovinskaia N et al. *Sci. Adv.* **2** (7) 12 (2016)
19. Dewaele A et al. *Nat. Commun.* **9** 2913 (2018)
20. Yagi T et al. *High Pressure Res.* **40** (1) 148 (2020)
21. Fedotenko T et al. *Rev. Sci. Instrum.* **90** 104501 (2019)
22. Troyan I et al. *Science* **351** 1303 (2016)
23. Drozdov A P et al. *Nature* **569** 528 (2019)
24. Bassett W A *Rev. Sci. Instrum.* **72** 1270 (2001)
25. Ming L C, Bassett W A *Rev. Sci. Instrum.* **45** 1115 (1974)
26. Prakapenka V B et al. *High Pressure Res.* **28** (3) 225 (2008)
27. Anzellini S, Boccato S *Crystals* **10** 28 (2020)
28. Heinz D L, Jeanloz R, in *High-Pressure Research in Mineral Physics* (Ed. Y Syono) (Washington, DC: American Geophysical Union, 1987) p. 113
29. Kavner A, Nugent C *Rev. Sci. Instrum.* **79** 024902 (2008)
30. Kavner A, Panero W R *Phys. Earth Planet. Interiors* **143–144** 527 (2004)
31. Burgress K et al. *Ultrasonics* **54** 963 (2014)
32. Zinin P V et al. *Rev. Sci. Instrum.* **87** 123908 (2016)
33. Campbell A J *Rev. Sci. Instrum.* **79** 015108 (2008)
34. Zinin P V et al. *High Pressure Res.* **39** 131 (2019)
35. Draper N R, Smith H *Applied Regression Analysis* (New York: Wiley, 1966)
36. Du Z X et al. *Rev. Sci. Instrum.* **84** 075111 (2013)
37. Deng J et al. *J. Appl. Phys.* **121** 025901 (2017)
38. Deemyad S, Papathanassiou A N, Silvera I F *J. Appl. Phys.* **105** 093543 (2009)
39. Rainey E S G, Hernlund J W, Kavner A *J. Appl. Phys.* **114** 204905 (2013)
40. Machikhin A S et al. *Opt. Lett.* **41** 901 (2016)
41. Pustovoit V I et al. *Proc. SPIE* **5953** 59530P (2005)
42. Magunov A N *Instrum. Exp. Tech.* **52** 451 (2009); *Prib. Tekh. Eksp.* (4) 5 (2009)
43. Jamieson J C, Lawson A W, Nachtrieb N D *Rev. Sci. Instrum.* **30** 1016 (1959)
44. Weir C E et al. *J. Res. Natl. Bureau Stand. A* **6** (1) 55 (1959)
45. Syassen K *High Pressure Res.* **28** (2) 75 (2008)
46. Piermarini G J et al *J. Appl. Phys.* **46** 2774 (1975)
47. Zou G T et al. *Rev. Sci. Instrum.* **72** 1298 (2001)
48. Jephcoat A P, Besedin S P *Philos. Trans. R. Soc. Lond. A* **354** 1333 (1996)
49. Bulatov K M et al. *J. Phys. Conf. Ser.* **1636** 012034 (2020)
50. Mazur M M et al. *Opt. Spectrosc.* **81** 475 (1996); *Opt. Spektrosk.* **81** 521 (1996)
51. Balakhov I V, Korobov V K, Pustovoit V I "Method of the color temperature measurement", USSR Patent (1972), http://www.findpatent.ru/patent/101/1012038.html
52. Kozlova O et al. *Rev. Sci. Instrum.* **87** 125101 (2016)
53. Machikhin A S et al. *Instrum. Exp. Tech.* **60** 401 (2017); *Prib. Tekh. Eksp.* (3) 100 (2017)
54. Machikhin A S, Zinin P V, Shurygin A V *Phys. Procedia* **70** 733 (2015)
55. Balakshii V I, Parygin V N, Chirkov L E *Fizicheskie Osnovy Akustooptiki* (Physical Foundations of Acustopics) (Moscow: Radio i Svyaz', 1985)
56. Goutzoulis A P, Pape D R (Eds) *Design and Fabrication of Acousto-Optic Devices* (New York: M. Dekker, 1994)
57. Magunov A N *Instrum. Exp. Tech.* **53** 910 (2010); *Nauch. Priborostroenie* **20** (3) 22 (2010)
58. Ribaud G *Traite De Pyrometrie Optique* (Paris: De La Revue, 1931)
59. Giampaoli R et al. *High Pressure Res.* **38** 250 (2018)
60. Mantrova Yu V et al. *J. Opt. Technol.* **87** 642 (2020); *Opt. Zh.* **87** (11) 10 (2020)
61. Taylor J *An Introduction to Error Analysis* (Mill Valley, CA: Univ. Science Books, 1982); Translated into Russian: *Vvedenie v Teoriyu Oshibok* (Moscow: Mir, 1985)
62. Bulatov K M et al. *Comput. Opt.* **41** 864 (2017)
63. Bykov A A et al. *J. Phys. Conf. Ser.* **946** 012085 (2018)
64. Mantrova Y V et al. *J. Phys. Conf. Ser.* **1421** 012060 (2019)
65. Bulatov K M et al. *High Pressure Res.* **40** 315 (2020)
66. Bulatov K M et al. *C. R. Geosci.* **351** (2–3) 286 (2019)
67. Bykov A et al. *J. Phys. Conf. Ser.* **1421** 012031 (2019)
68. Liu H W et al. *Measurement Sci. Technol.* **27** (2) 10 (2016)
69. Jyothi J et al. *Solar Energy Mater. Solar Cells* **171** 123 (2017)
70. Rozenbaum O et al. *Rev. Sci. Instrum.* **70** 4020 (1999)
71. Honner M et al. *Appl. Thermal Eng.* **94** 76 (2016)
72. Du Zh et al. *Rev. Sci. Instrum.* **84** 075111 (2013)
73. Pujana J et al. *Measurement Sci. Technol.* **18** 3409 (2007)
74. Boehler R *Hyperfine Interactions* **128** (1–3) 307 (2000)
75. Salem R et al. *Rev. Sci. Instrum.* **86** 093907 (2015)
76. Errandonea D et al. *Phys. Rev. B* **63** 132104 (2001)
77. Boehler R *Nature* **363** 534 (1993)
78. Bulatov K M, Zinin P V, Bykov A A *J. Surf. Investig. X-Ray, Synchrotron Neutron Tech.* **14** 1092 (2020)